


## Polymorphism of two-dimensional antiferromagnets, $\text{AgF}_2$ and $\text{CuF}_2$

Daniel Jeziński<sup>\*</sup> and Wojciech Grochala<sup>†</sup>

Center of New Technologies, University of Warsaw, 02089 Warsaw, Poland

 (Received 9 November 2023; accepted 27 February 2024; published 26 March 2024)

We present a theoretical study of relative stability, as well as of the magnetic and electronic properties, of  $\text{AgF}_2$  and  $\text{CuF}_2$ , in two related structural forms: orthorhombic (ambient pressure form of  $\text{AgF}_2$ ) and monoclinic (ambient pressure form of  $\text{CuF}_2$ ), using density functional theory. We demonstrate that the  $P2_1/c \rightarrow Pbcn$  structural transition is associated with a weakening of the intrasheet magnetic superexchange ( $|J_{2D}|$ ). This finding aligns with the flattening of two-dimensional (2D) layers, a smaller charge-transfer energy, and a stronger admixing of  $\text{Ag}_d/\text{Cu}_d$ - $F_p$  states in the monoclinic structure, compared to the orthorhombic form. Consequently, monoclinic  $\text{AgF}_2$  should be targeted in experiments as it is likely to exhibit stronger magnetic coupling than its orthorhombic counterpart. The dynamically stable  $P2_1/c$  form of  $\text{AgF}_2$  could be achieved through two alternative paths: by applying negative strain or by rapidly quenching silver(II) difluoride from temperatures above 480 K to low temperatures.

DOI: [10.1103/PhysRevMaterials.8.034407](https://doi.org/10.1103/PhysRevMaterials.8.034407)

### I. INTRODUCTION

The most typical structure adopted by transition metal difluorides at ambient pressure is the rutile type (Fig. 1). For  $\text{TMF}_2$ , where TM (transition metal) = V, Mn, Fe, Co, Ni, Pd, Zn, difluorides crystallize in the tetragonal system  $P4_2/mnm$  space group [1–3]. The building blocks of this structure consist of nearly regular octahedra of fluorine atoms surrounding each metal ion (CN = 6, where CN is the coordination number), featuring both edge and corner sharing of F atoms. However, in the case of  $\text{CrF}_2$  [4] and  $\text{CuF}_2$  [5], the deformation of octahedra is pronounced, primarily due to the Jahn-Teller effect. Here, the elongation of apical M-F bonds leads to the lowering of symmetry, resulting in monoclinic structure ( $P2_1/c$ ). Another important structural type among metal difluorides is fluorite, with a cubic ligand environment around the metal cation (CN = 8). Among TM systems, this type is adopted only by three difluorides: two with closed-shell cations,  $\text{CdF}_2$  and  $\text{HgF}_2$  (which could be classified as post-transition ones), and only one with an open  $d$ -shell cation,  $\text{AgF}_2$ . For the latter, the Jahn-Teller effect drives the distortion from the parent cubic polytype towards the orthorhombic one ( $Pbca$ ) [6]. Thus, both  $\text{CuF}_2$  and  $\text{AgF}_2$  exemplify the unique low-symmetry structure types, otherwise unknown among ionic fluorides.

Polymorphism of metal difluorides is even richer at elevated pressure conditions [3,7–10], as extensively studied during the last decade [11–14] (see also references in the Supplemental Material [15], i.e., Refs. [16–21] therein). Most TM difluorides adopt the close-packed cotunnite ( $Pnma$ ) structure (CN = 9) upon compression, with  $\text{Ni}_2\text{In}$ -type structure (CN = 11) as the ultimate high-pressure form. For instance,

$\text{FeF}_2$  undergoes the following sequence of phase transitions: rutile  $\rightarrow \text{CaCl}_2 \rightarrow \text{Ni}_2\text{In}$ , thus increasing the CN of the metal atom from 6 through 9 to 11. Another example is  $\text{NiF}_2$ , where compression up to 3 GPa induces a rutile  $\rightarrow \text{CaCl}_2$  transformation [10]. However, a theoretical study predicts that at 30 GPa, this compound should adopt a monoclinic structure ( $C2/c$ ), a hypothesis yet to be verified experimentally [17]. Additionally, there are two examples of difluorides where cotunnite structure has not been observed experimentally. The first is  $\text{PdF}_2$  (with high-spin  $d^8$  cations), where rutile  $\rightarrow$  cubic ( $Pa\bar{3}$ ) transformation occurs at 1.5 GPa [3]; this cubic polytype can also be stabilized in a low-temperature regime [22]. The second example is  $\text{AgF}_2$ , which undergoes the following transitions:  $Pbca \rightarrow Pca2_1 \rightarrow Pbcn \rightarrow Pnma$  [13], with two unusual intermediate forms: a noncentrosymmetric  $Pca2_1$  one and a unique nanotubelike  $Pbcn$ . A similar sequence is theoretically predicted for its lighter congener,  $\text{CuF}_2$  [11]. Indeed, the  $P2_1/c \rightarrow Pbcn$  ( $\text{AgF}_2$ -type) transition was observed for  $\text{CuF}_2$  at 9 GPa, while the  $\text{PbCl}_2$ -type structure is predicted theoretically to occur only at 72 GPa [11]. Clearly,  $\text{CuF}_2$  and  $\text{AgF}_2$  behave quite differently from the rest of the TM difluoride herd. Hence, studying polymorphism of these two rather poorly researched and unique fluorides is of interest.

Polymorphism significantly influences key material properties, such as, e.g., magnetic and electronic characteristics. We observe that both  $\text{AgF}_2$  and  $\text{CuF}_2$  are layered, with corrugated sheets composed of  $[\text{MF}_4]$  units (Fig. 2). However, the disparate stacking of sheets and the distinct nature of M-F bonds in both compounds (more covalent in Ag, more ionic in Cu) profoundly affect their physicochemical properties. Silver difluoride, in many aspects, resembles undoped oxocuprates (high-temperature superconductor (HTSC) precursors) [23–25]. Diverse methods of doping silver difluoride have been explored both theoretically [26–30] and experimentally [31]. As a result, we have recently observed the

<sup>\*</sup>d.jeziński@cent.uw.edu.pl

<sup>†</sup>w.grochala@cent.uw.edu.pl

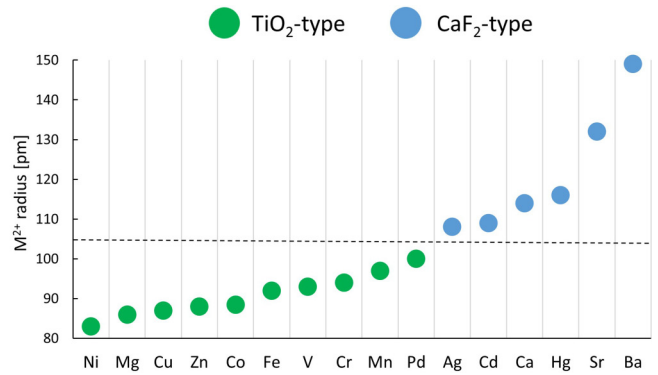
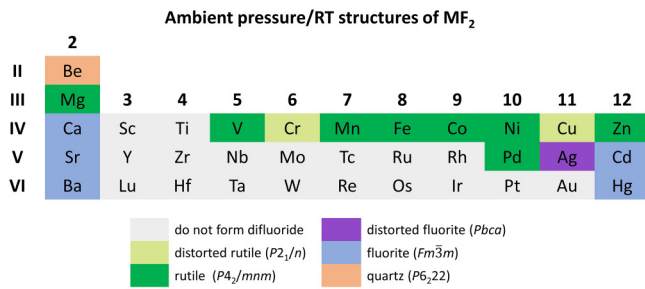


FIG. 1. Ambient pressure/room temperature structure of selected MF<sub>2</sub> (left) and type of structure adopted of binary difluorides depending on the  $M^{2+}$  ionic radius in octahedral environment (right). The dashed line indicates the boundary between two structure types, rutile and fluorite, the transition between the two being consistent with the Pauling ion packing rules.

coexistence of two structural types of solid solutions in Cu-Ag-F phase diagram: monoclinic (CuF<sub>2</sub> type) and orthorhombic (parent AgF<sub>2</sub> type; Fig. 2) [31]. Their formation is unexpected, considering the substantial difference in the cation size ( $R_{Cu^{2+}} = 0.87 \text{ \AA}$  and  $R_{Ag^{2+}} = 1.08 \text{ \AA}$ ) across the rutile/fluorite boundary (Fig. 1). Interestingly, under the experiment conditions discussed in Ref. [31], as much as 44% of Ag could be doped into the CuF<sub>2</sub> structure, and up to 30% Cu into the AgF<sub>2</sub> type. The formation of mixed-cation phases raises a pertinent question: could Cu-free AgF<sub>2</sub> be obtained in the monoclinic form, or Ag-free CuF<sub>2</sub> in the orthorhombic form, and what would be the key properties of these polymorphs? The experimental results suggest that CuF<sub>2</sub> may indeed be transformed into AgF<sub>2</sub> type at elevated pressure [9], but it remains unknown whether this high-pressure type can be quenched to ambient ( $p, T$ ) conditions, and what its properties would be. Conversely, whether AgF<sub>2</sub> can be obtained in the CuF<sub>2</sub> type remains an open question. These questions are important, since new polymorphic forms could constitute even more strongly magnetically coupled and thus better precursors of HTSC than the pristine ones.

Motivated by these findings, in this paper we theoretically study the dynamic and thermodynamic stability of four phases, i.e., CuF<sub>2</sub> and AgF<sub>2</sub>, each in two different structural types. We evaluate their key electronic and magnetic properties. Finally, we propose a possible experimental pathway to obtain the Cu-free monoclinic AgF<sub>2</sub>.

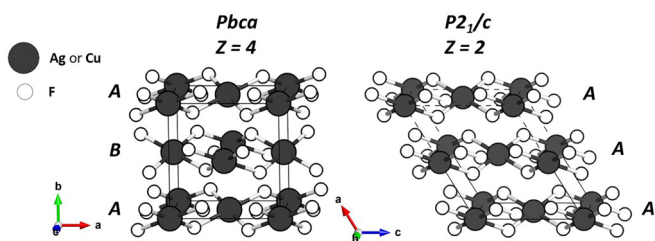


FIG. 2. The ambient pressure structures of AgF<sub>2</sub>  $Pbca$  (left) and CuF<sub>2</sub>  $P2_1/c$  (right). Only intralayer M-F bonds are shown for clarity. ABA and AAA marks refer to the type of layer stacking. In the case of the  $P2_1/c$  structure, a  $1 \times 2 \times 1$  supercell is presented for direct comparison with the orthorhombic structure.

## II. METHODS

Calculations were performed within the density functional theory (DFT) approach as implemented in the VASP 5.4.4 code [32], using a generalized gradient approximation type PBEsol [33] functional with projected augmented wave method [34,35]. The on-site Coulombic interactions of  $d$  electrons were realized by introducing Hubbard ( $U_d$ ) and Hund ( $J_H$ ) parameters (DFT+ $U$  formalism), as proposed by Liechtenstein [36]. In DFT+ $U$  and DFT+ $U$ +vdW methods, the  $J_H$  was set to 1 eV [37], while the  $U_d$  value was set to 8 and 10 eV, respectively, for Ag and Cu [24,38], where a van der Waals (vdW) dispersion energy-correction term was provided following the expression introduced by Grimme *et al.* (DFT-D3) [39]. Two other methods have also been employed: Strongly constrained and appropriately normed method (SCAN) and HSE06. A plane-wave cutoff energy of 520 eV was used in all systems. The  $k$  spacing was set to  $0.032 \text{ \AA}^{-1}$  for geometry optimization and  $0.022 \text{ \AA}^{-1}$  for self-consistent-field convergence. The convergence thresholds of  $10^{-7}$  eV for electronic and  $10^{-5}$  ionic steps were used. Calculations of phonon curves for each structure were realized using the PHONOPY package [40] (the step-by-step procedure is available online, on the official website). Zero-point energies/ $\Gamma$ -point frequencies, were calculated using density functional perturbation theory or finite differences approaches provided by VASP software.

## III. RESULTS AND DISCUSSION

### A. Structural features of silver and copper difluorides in both polymorphic forms

AgF<sub>2</sub> in its  $Pbca$  type, the first coordination sphere of cation, can be described as a deformed rhombic prism ( $2+2+2+2$  coordination), while CuF<sub>2</sub> in its parent  $P2_1/c$  structure, can be described as an elongated octahedron ( $4+2$  coordination; Fig. 3).

Our theoretical calculations accurately reproduce experimental structural parameters of AgF<sub>2</sub> and CuF<sub>2</sub> in their most stable structures (Table I). The best agreement between experimental and theoretical volumes of the unit cell was achieved using the SCAN method. The fully optimized AgF<sub>2</sub> and CuF<sub>2</sub> unit cells differ in volume from the experimental ambient pressure forms only by 1.75% and 1.66%, respectively [6,41].

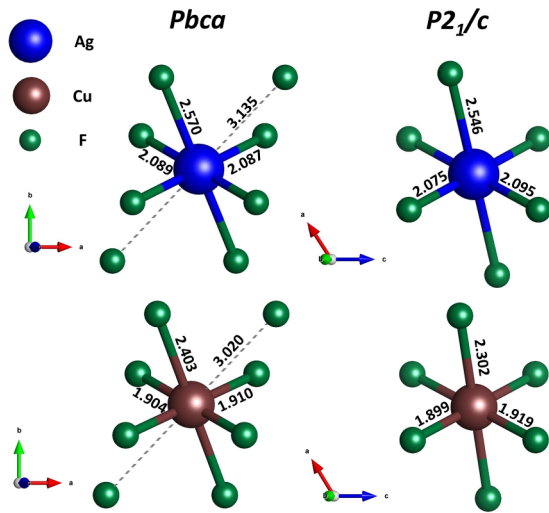


FIG. 3. First coordination sphere for  $\text{AgF}_2$  (up) and  $\text{CuF}_2$  (down) in  $Pbca$  (left) and  $P2_1/c$  (right) cells. The M-F bond lengths are expressed in Å, following SCAN calculations.

Comparable results come from the HSE06 method, where the volumes differ by 1.67% and 1.96%, respectively, for silver and copper difluoride compared to experimental data. However, the DFT+ $U$  method with van der Waals correction yields less accurate agreement—the volumes of optimized unit cells are underestimated by 5.51% and 7.02% compared to experimental ones, for  $\text{AgF}_2$  and  $\text{CuF}_2$ , respectively. These discrepancies are expected, as all calculations refer to conditions of  $T \rightarrow 0$  K and  $p \rightarrow 0$  atm and are partly due to the limitations of these theoretical methods. It is noted that adjusting the  $U$  and  $J$  values used in the spin-polarized DFT calculations may lead to better compatibility between experimental and theoretical structural parameters. This is supported by the works of Tokár *et al.* [42] and Kurzydłowski [11], where in DFT+ $U$  calculations,  $U_{\text{Ag}} = 5$  and  $J_{\text{Ag}} = 1$  for  $\text{AgF}_2$  and  $U_{\text{Cu}} = 7$  and  $J_{\text{Cu}} = 0.9$  eV for  $\text{CuF}_2$ , respectively, provide satisfactory agreement with experimental data.

Now, let us discuss the key structural differences between the  $Pbca$  and  $P2_1/c$  structure types. There are *three* main structural distinctions: (1) a different stacking of  $[\text{MF}_4]$  plaquettes,

i.e., ABA vs AAA (Fig. 1); (2) a reduction of coordination number for  $M^{2+}$  ions from 8 to 6; and (3) accompanying changes in bond lengths and bond angles. According to SCAN calculations, four intralayer (equatorial) Ag-F bond lengths in  $\text{AgF}_2$  are similar:  $2 \times 2.087$  and  $2 \times 2.089$  Å. The apical (axial) bonds are considerably longer:  $2 \times 2.570$  Å. The last Ag-F contacts, which complete the  $\text{Ag}^{2+}$  first coordination sphere, are significantly longer than the others:  $2 \times 3.135$  Å. Similarly, in the  $Pbca$  structure of  $\text{CuF}_2$ , the first coordination sphere of the cation includes the shortest contacts of  $2 \times 1.904$  and  $2 \times 1.910$  Å, the apical ones of  $2 \times 2.403$  Å, and secondary interactions at  $2 \times 3.020$  Å.

In the  $P2_1/c$  system, the coordination sphere of the  $M^{2+}$  ion is sixfold (CN = 6; Fig. 2). For  $\text{AgF}_2$  in this structure, two intralayer Ag-F contacts are marginally shorter and two are slightly longer compared to those in the  $Pbca$  structure:  $2 \times 2.075$  and  $2 \times 2.095$  Å. The apical bond lengths exhibit a larger difference:  $2 \times 2.546$  Å in the  $P2_1/c$  form compared to  $2 \times 2.570$  and  $2 \times 3.135$  Å in the  $Pbca$  form. This indicates that the apical bonds are shorter in the monoclinic form, consistent with the reduction in the coordination number of the cation. In the case of  $\text{CuF}_2$ , the intralayer copper-fluoride bonds in the  $P2_1/c$  form are 1.899 and 1.919 Å, while the apical contacts are notably shorter in this form ( $2 \times 2.302$  Å) compared to the  $Pbca$  form ( $2 \times 2.403$  Å +  $2 \times 3.020$  Å). This observation aligns with the results previously reported by Kurzydłowski [11]. The results from all computational methods indicate similar tendencies of bond length changes despite slight differences in absolute values [Supplemental Material (SM) Tables SI 1 and SI 2 [15]].

Puckering of the  $\text{MF}_2$  layers is also different in both structure types. For example, for the monoclinic  $\text{AgF}_2$ , the intralayer Ag-F-Ag angle is larger by  $\sim 1.2^\circ$  than for the orthorhombic one (SCAN). For  $\text{CuF}_2$  the effect is even more pronounced ( $3.0^\circ$ ). This may be related to the different metal-metal distances in both structures. In the  $P2_1/c$  system the Ag-Ag intralayer distance is larger by 0.3%, whereas the interlayer contact is shorter by 2.8% compared to the  $\text{AgF}_2$   $Pbca$  form. For copper difluoride, the intralayer Cu-Cu distance is 1.3% larger, whereas the interlayer one is 8.0% shorter for the  $P2_1/c$  form (all values are listed in Table SI1-2 in the SM [15]). All these features impact, as we will see, the magnetic and electronic properties of both polymorphs.

TABLE I. Unit-cell parameters  $a$ ,  $b$ ,  $c$ , volumes  $V$  per formula unit (f.u.) as estimated from experimental measurements [x-ray and neutron powder diffraction (XRPD and NPD)] with theoretical values from our calculations for orthorhombic  $\text{AgF}_2$  and monoclinic  $\text{CuF}_2$  (for antiferromagnetic spin ground state). For the orthorhombic cell all unit-cell angles are equal to  $90^\circ$ , whereas for the monoclinic one  $\alpha = \gamma = 90^\circ \neq \beta$ .

Method	$\text{AgF}_2$ ( $Pbca$ )				Method	$\text{CuF}_2$ ( $P2_1/c$ )				
	$a$ (Å)	$b$ (Å)	$c$ (Å)	V/f.u. (Å <sup>3</sup> )		$a$ (Å)	$b$ (Å)	$c$ (Å)	$\beta$ [°]	V/f.u. (Å <sup>3</sup> )
XRPD, RT [31]	5.550	5.836	5.095	41.257	XRPD, RT [31]	3.294	4.559	5.345	121.11	34.704
NPD, 4.2 K [6]	5.524	5.780	5.066	40.438	NPD, 4.2 K [41]	3.294	4.568	5.358	121.17	34.491
XRD, RT [43]	5.568	5.831	5.101	41.403	XRPD, RT [11]	3.302	4.560	5.352	121.11	34.497
DFT+ $U$	5.433	5.768	5.008	39.234	DFT+ $U$	3.192	4.505	5.293	121.32	32.510
DFT+ $U$ +vdW	5.408	5.660	4.993	38.211	DFT+ $U$ +vdW	3.185	4.479	5.286	121.72	32.068
SCAN	5.583	5.724	5.151	41.145	SCAN	3.302	4.522	5.310	121.20	33.917
HSE06	5.539	5.843	5.082	41.115	HSE06	3.296	4.516	5.300	120.98	33.817

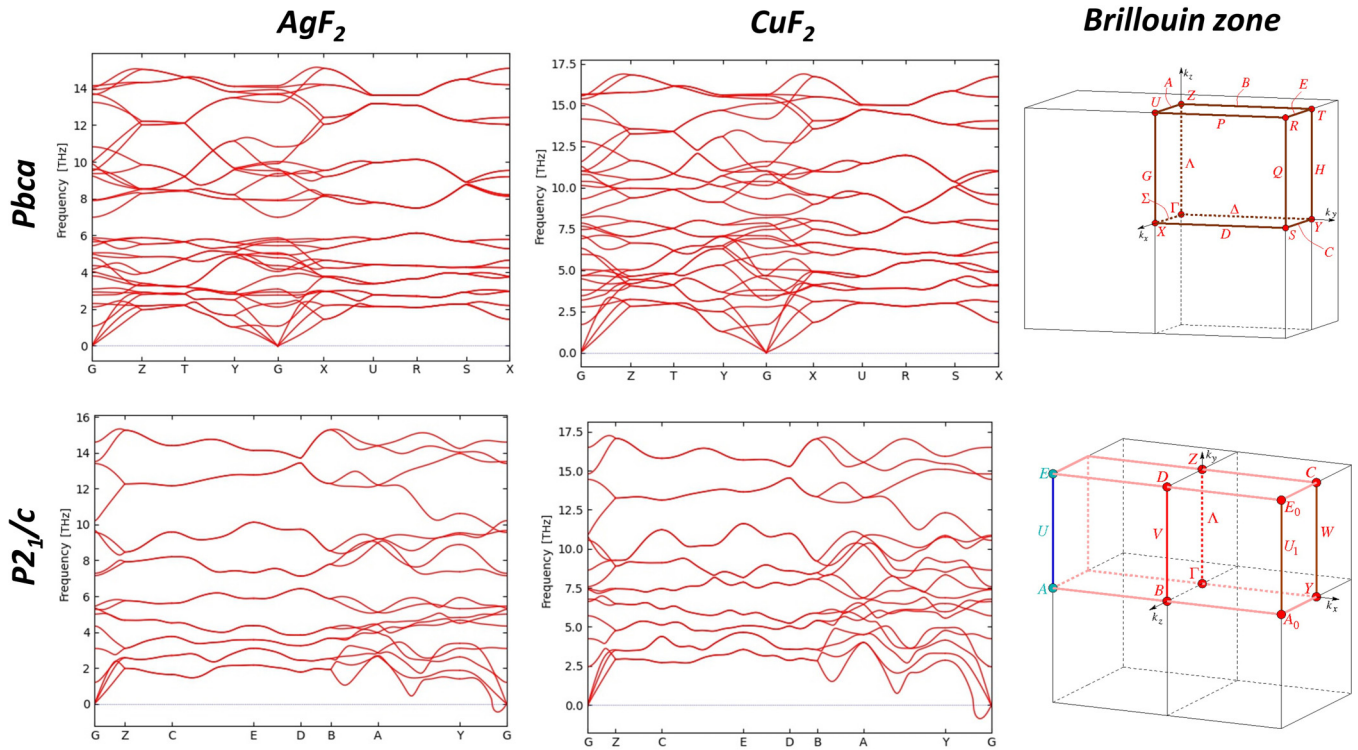


FIG. 4. Phonon dispersion curves for  $\text{AgF}_2$  (left) and  $\text{CuF}_2$  (right) in  $Pbca$  (upper) and  $P2_1/c$  systems (down). The Brillouin zones for both crystal systems were taken from Bilbao Crystallographic Server [62].

### B. Dynamic stability

To evaluate dynamic stability, we calculated the phonon modes at the gamma point for  $\text{AgF}_2$  and  $\text{CuF}_2$  in both polymorphic forms:  $Pbca$  and  $P2_1/c$  (Table II, and Tables SI7–SI11 of the SM). Experimental (IR, Raman) and theoretical phonon frequencies of  $\text{AgF}_2$  ( $Pbca$ ) with their symmetry and optical activity, have been previously reported by Gawraczyński *et al.* [23]. Additionally, Kurzydłowski [11] previously assigned Raman-active bands of  $\text{CuF}_2$  ( $P2_1/c$ ). Here, we extended this assignment to IR-active  $\text{CuF}_2$  bands of the monoclinic form. Additionally, we calculated the dispersion of phonons for binary difluorides at  $P2_1/c$  and  $Pbca$  structures in the DFT+ $U$  framework (Fig. 4).

Analysis of phonon dispersion curves (Fig. 4) shows no dynamic instability for both compounds in the orthorhombic system ( $Pbca$ ). However, in monoclinic form ( $P2_1/c$ ), both compounds show very small soft features at  $q = (-0.04, 0.04, -0.04)$ . This obviously is not exact point in reciprocal space, and indeed, geometry optimization of the structures obtained following the said imaginary mode does not lead to lower energy (Table SI6 in SM [15]). In other words, tiny imaginary features off the zone center are purely artifactual. The lack of genuine imaginary modes suggests that monoclinic  $\text{AgF}_2$  and orthorhombic  $\text{CuF}_2$  are local minima at the potential energy surface, and they could, in principle, be observed at  $T \rightarrow 0$  K and  $p \rightarrow 0$  GPa.

On the basis of group theory, for the  $P2_1/c$  structure ( $Z = 2$ ), among the 18  $\Gamma$ -point optical modes, 9 are IR active ( $5A_u + 4B_u$ ) and 6 are Raman active ( $3A_g + 3B_g$ ). For the  $Pbca$  structure, group theory predicts that 15 modes are

IR active ( $5B_{1u} + 5B_{2u} + 5B_{3u}$ ), 12 are Raman active ( $3A_g + 3B_{1g} + 3B_{2g} + 3B_{3g}$ ), and 6 are silent ( $A_u$ ). The theoretical results obtained from all theoretical methods used in this work are presented in the Supplemental Material (SM Tables SI8–SI11 [15]). Here we show the theoretical frequencies of the modes, and their symmetry and activity, following DFT+ $U$ +vdW results only (Table II).

The good agreement between theoretical and experimental values of the mode frequencies reflects the precision of the DFT method (SM Table SI7 [15]). Moreover, translations (acoustic modes) are computed with a  $\pm 2 \text{ cm}^{-1}$  error bar, suggesting that optical frequencies may have a similarly small error.

Raman and IR spectroscopies are exceptionally powerful tools for detecting structural transitions in compounds, as they provide insight into the local environment of atoms and can be easily combined with equipment such as a diamond anvil cell, commonly used in high-pressure studies. Therefore, analyzing Raman and IR spectra could be instrumental in revealing a potential structural transition of  $\text{AgF}_2$ . To predict changes in the spectra during such transitions, we will now analyze both IR- and Raman-active modes for  $\text{AgF}_2$ , as well as for  $\text{CuF}_2$  in both structural forms. It is noteworthy that the evolution of Raman spectra of  $\text{CuF}_2$  under pressure has recently been used to detect the  $P2_1/c \rightarrow Pbca$  transition [11]. Thus, this work complements previous research by including data on IR-active modes for this compound in both its structural forms.

Based on Table II, clear differences are evident in the fundamental phonons between  $\text{AgF}_2$  and  $\text{CuF}_2$  in their two polymorphic forms. The symmetry-related modes (e.g.,  $B_{1g}$

TABLE II. The list of  $\Gamma$ -point frequencies of the  $\text{AgF}_2$  and  $\text{CuF}_2$  compounds in  $Pbca$  and  $P2_1/c$  structures (DFT+ $U$ +vdW). Activity of modes in parentheses. Shaded columns correspond to the translational modes. Frequency in  $\text{cm}^{-1}$ .

<i>Pbca</i>				<i>P2<sub>1</sub>/c</i>			
No.	$\text{AgF}_2$ ( $\text{cm}^{-1}$ )	$\text{CuF}_2$ ( $\text{cm}^{-1}$ )	Symm. (activity)	No.	$\text{AgF}_2$ ( $\text{cm}^{-1}$ )	$\text{CuF}_2$ ( $\text{cm}^{-1}$ )	Symm. (activity)
1	478	526	$B_{1g}$ (Raman)	1	493	560	$B_g$ (Raman)
2	475	524	$B_{2g}$ (Raman)	2	453	490	$B_u$ (IR)
3	473	528	$A_u$ (silent)	3	452	500	$A_u$ (IR)
4	467	511	$B_{1u}$ (IR)	4	355	389	$A_g$ (Raman)
5	464	518	$B_{3u}$ (IR)	5	333	373	$A_u$ (IR)
6	450	476	$B_{2u}$ (IR)	6	326	357	$B_u$ (IR)
7	369	432	$B_{2u}$ (IR)	7	241	294	$B_g$ (Raman)
8	347	395	$A_u$ (silent)	8	240	263	$A_g$ (Raman)
9	332	388	$B_{3g}$ (Raman)	9	183	250	$B_u$ (IR)
10	329	372	$B_{1u}$ (IR)	10	180	254	$A_u$ (IR)
11	325	371	$B_{3u}$ (IR)	11	175	235	$B_g$ (Raman)
12	324	369	$B_{3g}$ (Raman)	12	158	220	$A_u$ (IR)
13	307	347	$A_g$ (Raman)	13	149	192	$B_u$ (IR)
14	274	318	$B_{1g}$ (Raman)	14	108	145	$A_u$ (IR)
15	273	357	$B_{2g}$ (Raman)	15	54	75	$A_g$ (Raman)
16	240	242	$A_g$ (Raman)	16	0	0	$B_u$
17	203	267	$B_{3u}$ (IR)	17	0	2	$A_u$
18	197	261	$B_{1u}$ (IR)	18	1	1	$B_u$
19	191	254	$A_u$ (silent)				
20	186	283	$B_{1g}$ (Raman)				
21	172	231	$A_u$ (silent)				
22	172	236	$B_{2u}$ (IR)				
23	165	203	$B_{2u}$ (IR)				
24	148	172	$B_{3u}$ (IR)				
25	148	160	$B_{1u}$ (IR)				
26	137	157	$B_{2g}$ (Raman)				
27	136	231	$B_{3g}$ (Raman)				
28	114	160	$A_u$ (silent)				
29	105	126	$B_{2u}$ (IR)				
30	99	113	$B_{3u}$ (IR)				
31	90	104	$A_u$ (silent)				
32	79	180	$A_g$ (Raman)				
33	45	71	$B_{1u}$ (IR)				
34	0	1	$B_{2u}$				
35	1	2	$B_{1u}$				
36	1	1	$B_{3u}$				

in both compounds in orthorhombic form), exhibit higher frequencies in the case of copper difluoride. In the simplest harmonic approximation, the vibration energy is proportional to the bonding strength (force constant) and inversely proportional to the mass of interacting atoms (reduced mass). Although, the M-F bond is more covalent in  $\text{AgF}_2$  than in  $\text{CuF}_2$  [24,43–45], it appears that the reduced mass is the dominant factor influencing the observed changes in mode frequencies; the mass of Cu constitutes only  $\sim 60\%$  of the atomic mass of Ag.

Regarding the experimentally-related issue, transition from monoclinic to orthorhombic structure of  $\text{AgF}_2$  should be accompanied with reduction of the number of band appearing in both IR and Raman spectra, from 27 to 15 optically active modes. Additionally,  $Pbca \rightarrow P2_1/c$  transition should be reflected in the changes of the frequencies of symmetry-related modes. For instance, the sudden change of 15–18  $\text{cm}^{-1}$

is expected, between symmetry-related  $B_{1g}$  (478  $\text{cm}^{-1}$ ) and  $B_{1g}$  (475  $\text{cm}^{-1}$ ) modes for  $Pbca$  and  $B_g$  (493  $\text{cm}^{-1}$ ) for  $P2_1/c$  polymorphs. This trend of mode stiffening is more general, as the ZPE value is predicted to be higher by 7 meV/f.u. (Table III) for  $P2_1/c$  form, than that, for the ambient pressure form of silver difluoride. This emerges partially from the changes in the average value of associated bond lengths. Based on the theoretical results, the shortening by approx. 0.1% and 0.9%, for equatorial and axial M-F bonds, respectively, following  $Pbca \rightarrow P2_1/c$  transformation, should indeed take place for  $\text{AgF}_2$ . Same trend holds for  $\text{CuF}_2$ .

### C. Energetic and thermodynamic stability of both polymorphs

Comparing ground state energies of binary fluorides in  $P2_1/c$  and  $Pbca$  systems (including zero-point energies) and volume changes ( $dV$ ) arising from their structure modifica-

TABLE III. Ground state energies ( $E_{GS}$ ), volumes of unit cell ( $V$ ), zero-point energies (ZPE), transition pressure ( $p$ ) including zero-point energy ( $p_{ZPE}$ ), and transition temperature from ambient pressure structure without ( $T$ ) and with zero-point energy ( $T_{ZPE}$ ). Data within DFT+ $U$ +vdW methods Results from all methods presented in the Supplemental Material, Tables SI4 and SI5 [15].

AgF <sub>2</sub>	$E_{GS}/\text{f.u. (eV)}$	$V/\text{f.u. (Å}^3\text{)}$	ZPE (eV)	$p$ (GPa)	$p_{ZPE}$ (GPa)	$T$ (K)	$T_{ZPE}$ (K)
$P2_1/c$	-9.224	40.995	0.121	-2.8	-2.4	573	480
$Pbca$	-9.273	38.211	0.129				
CuF <sub>2</sub>	$E_{GS}/\text{f.u. (eV)}$	$V/\text{f.u. (Å}^3\text{)}$	ZPE (eV)	$p$ (GPa)	$p_{ZPE}$ (GPa)	$T$ (K)	$T_{ZPE}$ (K)
$P2_1/c$	-11.626	32.068	0.143	6.3	7.3	805	933
$Pbca$	-11.557	30.311	0.154				

tion, we may estimate the relative stability of both polymorphs as well as the transition pressure of  $P2_1/c \rightarrow Pbca$  transformation for both compounds. In doing so we follow equation  $p = \frac{dE}{dV}$  (1) and assume so-called common tangent approximation. The results obtained with the state-of-the-art DFT+ $U$ +vdW method are listed in Table III (for all methods tested, cf. Tables SI3 and SI4 in the SM [15]).

Copper difluoride in the  $Pbca$  structure is uphill by 80 meV per formula unit (f.u.) (including ZPE) as compared to monoclinic form; this explains the persistence of the latter in experiment at ambient ( $p, T$ ) conditions. However, the volume of the  $Pbca$  form is 1.65–1.76 Å<sup>3</sup> smaller than in the case of the monoclinic form, suggesting that orthorhombic form could be achieved at elevated pressure. Our computed transition pressure of 7.3 GPa is only slightly underestimated (experimental value is 1.7 GPa larger [11]).

In the case of AgF<sub>2</sub>, the relative stability of the two structures depends on the method used (as detailed in the SM [15]). Using the DFT+ $U$ +vdW standard, the  $Pbca$  form is more stable than the monoclinic form by 49 meV (including ZPE). Conversely, the unit-cell volume of AgF<sub>2</sub> in the  $Pbca$  form is approximately 1.7 Å<sup>3</sup> smaller than in  $P2_1/c$ . Therefore, according to Eq. (1), the calculated pressure for the transition must be negative. Our calculations yield a value of approximately -2.4 GPa with DFT+ $U$ +vdW (Table III). Given that the ambient ( $p, T$ ) form of AgF<sub>2</sub> is orthorhombic ( $Pbca$ ), the use of a van der Waals functional appears necessary for an accurate description of relative stability. However, the formally negative value of transition pressure, while unphysical, may be somewhat replicated by negative strain, such as in epitaxial deposition techniques. Furthermore, it is possible to estimate the temperature needed for a structural transition to occur. For silver difluoride, the estimated temperature for the  $Pbca \rightarrow P2_1/c$  structural transformation is approximately equal to 450 K (with ZPE correction). We will return to this finding below.

#### D. Electronic and magnetic properties

Figure 5 presents the electronic density of states for copper and silver difluorides in two structures:  $Pbca$  and  $P2_1/c$ . The value of the fundamental band gap, calculated for AgF<sub>2</sub> ( $Pbca$ ), is consistent within three methods used: DFT+ $U$ +vdW and HSE06, and equals ~2.17–2.18 eV (Table III). However, the SCAN method yields a severely underestimated value of band gap (BG) of 0.52 eV. Since the experimentally determined charge-transfer gap according

to the Zaanen-Sawatzky-Allen scheme [46] is ~3.4 eV [25], we conclude that even the HSE06 method underestimates the gap. For the monoclinic form of AgF<sub>2</sub> ( $P2_1/c$ ), the calculated charge-transfer gap is ~1.94–1.96 eV (within DFT+ $U$ +vdW and HSE06). These values are 11% smaller than the gap computed for the orthorhombic form so, given error canceling, we expect that the experimentally determined BG for monoclinic form would indeed be smaller than that for the orthorhombic form (89% of 3.4 eV yields ~3.0 eV).

Changes in the band-gap value associated with structural transformations are also observed in the case of CuF<sub>2</sub>. For the ambient pressure form of copper difluoride, the DFT+ $U$ +vdW method gives a BG of 4.46 eV, while HSE06 predicts a slightly smaller value of 4.14 eV. To the best of our knowledge, there is no experimental estimate of the band-gap value for CuF<sub>2</sub>. However, our theoretical results align with previously reported calculations by Miller and Botana [45]. It can be expected that the band gap for more ionic CuF<sub>2</sub> should indeed be larger than for more covalent AgF<sub>2</sub>. Again, as for AgF<sub>2</sub>, calculations predict a larger gap for the orthorhombic than for the monoclinic form (by 4% and 7%, following DFT+ $U$ +vdW and HSE06 results, respectively). To confirm these findings, the high-pressure form of CuF<sub>2</sub> should first be quenched to ambient ( $p, T$ ) conditions, and its band gap subsequently examined.

The results obtained for AgF<sub>2</sub> agree qualitatively with the maximum hardness principle by Pearson [47] as a broader gap ( $Pbca$ ) form is more stable (at  $p \rightarrow 0$  atm,  $T \rightarrow 0$  K) than a narrower gap ( $P2_1/c$ ) form. Interestingly, a contradictory observation can be made for CuF<sub>2</sub>.

The inspection of density of states (as presented in Fig. 5), reveals some differences in the contributions from silver and fluorine states to conduction and valence bands between  $P2_1/c$  and  $Pbca$  forms of AgF<sub>2</sub>. In the orthorhombic form of silver difluoride (ambient pressure), the valence band, particularly near the Fermi level, is predominantly composed of  $F_p$  states, while the conduction band [i.e., upper Hubbard band (UHB)] is mainly formed by  $Ag_d$  states. In the monoclinic form, one may note a stronger admixture of Ag and F states in both bands, suggesting enhanced covalency in Ag-F. This is consistent with the observed changes in bond lengths and optical phonon frequencies. A similar trend is even more evident in the case of CuF<sub>2</sub> (Fig. 5, bottom part). Here, again, the monoclinic form exhibits greater hybridization of  $Cu_d-F_p$  states than the orthorhombic one.

The width of the upper Hubbard band (conduction band), is another crucial parameter related to potential electron doping

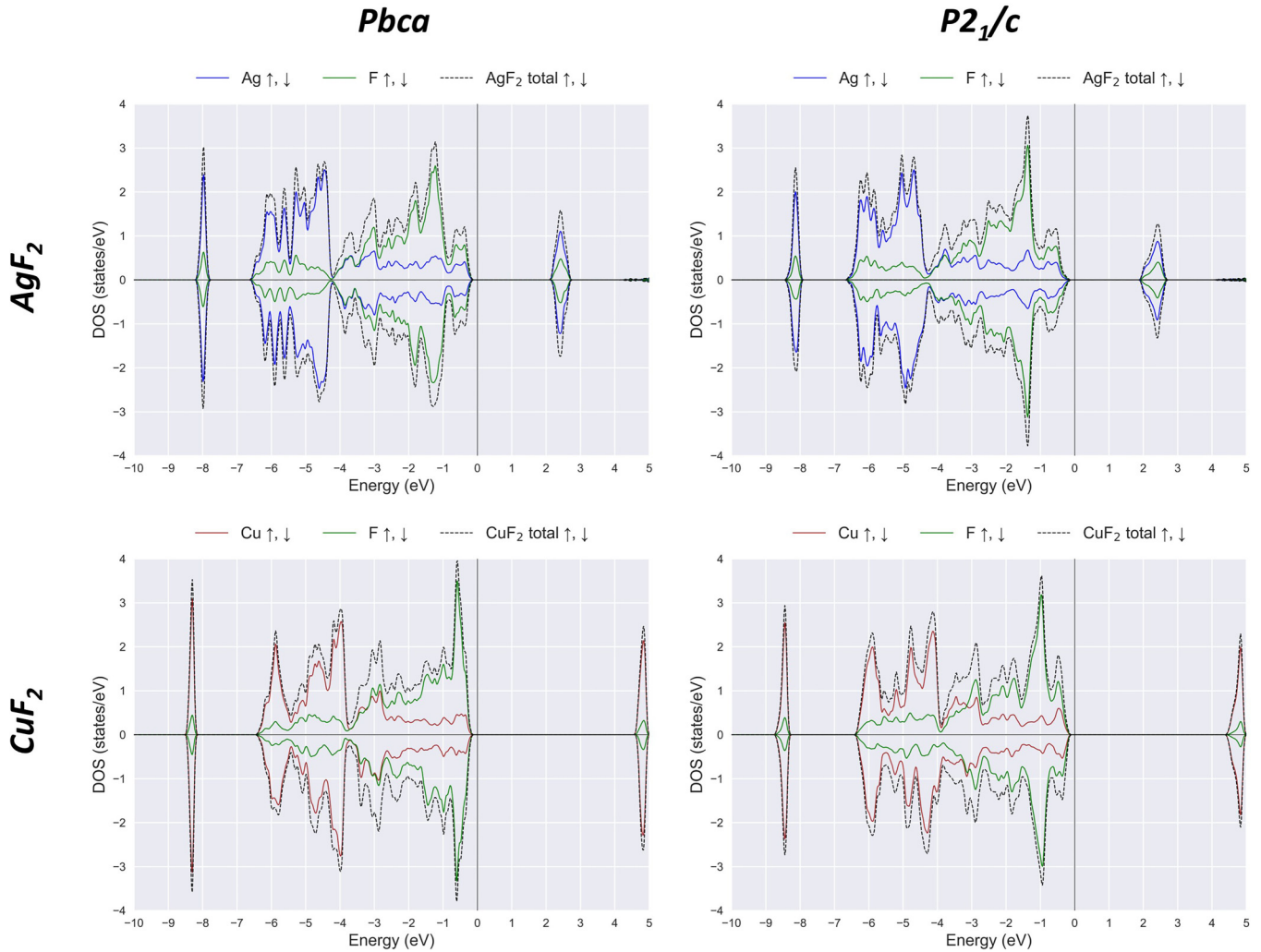


FIG. 5. Atom-resolved eDOS for  $\text{AgF}_2$  (upper) and  $\text{CuF}_2$  (lower) in  $Pbca$  and  $P2_1/c$  systems calculated within the DFT+ $U$ +vdW methods. For eDOS from the HSE06 method, please check Fig. S11 in the SM [15].

of both compounds [28,48]. Our results suggest that in both compounds, the UHB is slightly wider in the  $P2_1/c$  structure compared to the  $Pbca$  one. Consequently,  $\text{AgF}_2$  in the monoclinic structure might be more feasible to dope than in its ambient ( $p,T$ ) form [27].

As  $\text{AgF}_2$  and  $\text{CuF}_2$  are two-dimensional antiferromagnets (for  $\text{AgF}_2$ ,  $T_N = 163$  K [49], whereas for  $\text{CuF}_2$ ,  $T_N = 69$  K [50]), the strength of magnetic superexchange,  $J_{2D}$ , is of interest. The experimentally determined  $J_{2D}$  value for  $\text{AgF}_2$  is equal to  $\sim -70$  meV [23] (the negative sign indicates an antiferromagnetic interaction). The SCAN predicts a very similar value,  $-67.3$  meV; in the DFT+ $U$  method, the superexchange value is twice as low (Table IV). In the case of  $\text{CuF}_2$ , limited information is available on the experimentally determined value of the intrasheet magnetic superexchange constant. To the best of our knowledge, there is only one experimental paper, where authors claim the magnitude of  $J_{2D}$  to be  $-2.9$  meV [50], on the basis of magnetic measurements. However, a sophisticated computational method predicts it to be  $\sim -11$  meV [51]. Our calculations are not so far from the latter; DFT+ $U$ +vdW predicts a value of  $-8.2$  meV. On the

other hand, the SCAN and HSE06 methods predict a higher absolute value of  $J_{2D}$ , i.e.,  $-21.6$  and  $-18.3$  meV, respectively (Table IV). The exact superexchange constant value in DFT+ $U$  methods, strongly depends on the magnitude of the  $U$  and  $J$  parameters used [31,45]. Therefore, regarding the results from the DFT+ $U$ +vdW methods, we mainly focus on the changes of  $J_{2D}$  values between two polymorphs.

Our calculations reveal enhancement in the absolute values of  $J_{2D}$  for  $\text{AgF}_2$  in the  $P2_1/c$  form by 13%–19%, depending on the method used (Table IV and Table SI5). This trend is consistent in the case of  $\text{CuF}_2$  with an increase of 13%–20%. Such changes in the  $J_{2D}$  value are directly related to the alterations in M-M distances, and consequently, to the widening of the F-M-F angle driven by the structural transformation from  $Pbca$  to  $P2_1/c$ . In accordance with the Goodenough-Kanamori-Anderson [52–54] rules, a more effective orbital overlap is expected with the flattening of the F-M-F angle. Therefore, stronger hybridization of M-F orbitals leads to a higher absolute value of the antiferromagnetic  $J_{2D}$ . Given that the  $J_{2D}$  value is correlated with the maximum experimental superconducting critical temperature in doped cuprates [55],

TABLE IV. Band gaps, magnetic moments, and  $J_{2D}$  values for  $\text{AgF}_2$  and  $\text{CuF}_2$  in  $Pbca$  and  $P2_1/c$  structures, obtained using various calculation methods. Negative values of  $J_{2D}$  indicate antiferromagnetic interaction.

Method	System	$\text{AgF}_2$			$\text{CuF}_2$		
		BG (eV)	$\pm\mu_{\text{AFM}}$	$J_{2D}$ (meV)	BG (eV)	$\pm\mu_{\text{AFM}}$	$J_{2D}$ (meV)
DFT+ $U$	$Pbca$	2.18	0.66	-32.7	4.63	0.88	-6.6
	$P2_1/c$	1.95	0.67	-40.2	4.46	0.89	-8.2
DFT+ $U$ +vdW	$Pbca$	2.17	0.67	-31.9	4.64	0.88	-6.6
	$P2_1/c$	1.94	0.67	-39.4	4.46	0.89	-8.2
SCAN	$Pbca$	0.52	0.52	-67.3	1.58	0.75	-18.8
	$P2_1/c$	0.35	0.52	-81.0	1.21	0.76	-21.6
HSE06	$Pbca$	2.18	0.60	-54.7	4.46	0.81	-15.6
	$P2_1/c$	1.96	0.60	-63.2	4.14	0.81	-18.3

synthesis of the monoclinic  $\text{AgF}_2$  precursor is of significant interest.

Another intriguing aspect concerns the relationship between charge-transfer energy ( $\Delta_{\text{CT}}$ ) and the  $J_{2D}$  value. In the case of transfer insulators, electron hopping from the  $d$  orbital of a transition metal site to another, and back, involves the  $p$  orbital of a nonmetal. Consequently, the  $J$  value is proportional to  $1/(\Delta_{\text{CT}})^2$  [52–54,56]. Indeed, our results indicate that a larger  $|J_{2D}|$  is associated with a smaller  $\Delta_{\text{CT}}$ . This dependence remains consistent across all methods employed (Table IV; cf. SM [15]) for both compounds in  $Pbca$  and  $P2_1/c$  structures.

#### IV. CONCLUSIONS

In this paper, we employed various theoretical methods to investigate the structural, electronic, and magnetic properties of the known, high-pressure orthorhombic form of  $\text{CuF}_2$  ( $Pbca$ ) and the not-yet-achieved monoclinic form of  $\text{AgF}_2$  ( $P2_1/c$ ), comparing them with those of the ambient ( $p,T$ ) polymorphs. We found that both fluorides are dynamically stable in the monoclinic structure and exhibit a higher  $|J_{2D}|$  value, a smaller charge-transfer gap, and a wider UHB compared to the orthorhombic form. These findings are particularly significant in the case of  $\text{AgF}_2$ , which is perceived as an analog of cuprates. The stabilization of the monoclinic form of silver(II) difluoride ( $P2_1/c$ ) could be crucial for achieving the long-awaited doping of this compound.

Furthermore, there is increasing interest in the existence of a new type of magnetism—altermagnetism [57]. The discovery of altermagnetism has led to searches for compounds characterized by perfectly compensated magnetic order and nonrelativistic spin splitting [58,59]. In this area,  $\text{MnF}_2$  in the form of a two-dimensional monolayer [60] with colossal

spin splitting, has been recognized. Very recently,  $\text{AgF}_2$  has also been identified as a possible altermagnet, particularly if the exfoliation to a monolayer form with  $P2_1/c$  symmetry can be achieved [61]. The emerging research on altermagnets will show to what extent these predictions can be realized in practice.

Based on our theoretical findings, we suggest that the desired structural transition of  $\text{AgF}_2$  to monoclinic form could potentially be achieved in two ways, aside from partial Cu doping [31]: (1) under negative strain conditions [48], or (2) through heating to  $T > 480$  K followed by rapid quenching. In the case of the first method proposed, the interatomic Ag-Ag distance within the  $\text{AgF}_2$  layer could be controlled by lattice parameters of the substrate, thus ensuring proper strain for crystal growth of the  $P2_1/c$  polytype. For the second method, heating to 480 K should be conducted under fluorine gas overpressure to prevent thermal decomposition. Unfortunately, such rapid thermal quenching experiments have not yet been conducted for  $\text{AgF}_2$ .

#### ACKNOWLEDGMENTS

W.G. is grateful to the Polish National Science Center (NCN) for project Maestro (2017/26/A/ST5/00570). Research was carried out with the use of CePT infrastructure financed by the European Union—the European Regional Development Fund within the Operational Programme “Innovative economy” for 2007–2013 (POIG.02.02.00-14—024/08-00). Quantum mechanical calculations were performed using supercomputing resources of the ICM UW (project SAPPHERE GA83-34). The authors appreciate valuable comments from Professor Jose Lorenzana (CNR and La Sapienza, Rome, Italy).

[1] W. H. Baur, S. Guggenheim, and J. C. Lin, *Acta Cryst. B* **38**, 351 (1982).  
 [2] J. W. Stout and S. A. Reed, *J. Am. Chem. Soc.* **76**, 5279 (1954).  
 [3] A. Tressaud, J. L. Soubeyroux, H. Touhara, G. Demazeau, and F. Langlais, *Mater. Res. Bull.* **16**, 207 (1981).  
 [4] R. Maitland and K. Jack, *Proc. Chem. Soc.* **232** (1957).  
 [5] C. Billy and H. M. Haendler, *J. Am. Chem. Soc.* **79**, 1049 (1957).

[6] P. Charpin, P. Plurien, and P. Mériel, *Bull. Mineral.* **93**, 7 (1970).  
 [7] L. Ming and M. H. Manghnani, *Geophys. Res. Lett.* **5**, 491 (1978).  
 [8] G. Liu, H. Wang, Y. Ma, and Y. Ma, *Solid State Commun.* **151**, 1899 (2011).  
 [9] J. A. Barreda-Argüeso, S. López-Moreno, M. N. Sanz-Ortiz, F. Aguado, R. Valiente, J. González, F. Rodríguez, A. H. Romero, A. Muñoz, L. Nataf, and F. Baudelet, *Phys. Rev. B* **88**, 214108 (2013).



- [10] J. D. Jorgensen, T. G. Worlton, and J. C. Jamieson, *Phys. Rev. B* **17**, 2212 (1978).
- [11] D. Kurzydłowski, *Crystals* **8**, 140 (2018).
- [12] D. Kurzydłowski, A. Oleksiak, S. B. Pillai, and P. K. Jha, *Inorg. Chem.* **59**, 2584 (2020).
- [13] A. Grzelak, J. Gawraczyński, T. Jaroń, D. Kurzydłowski, A. Budzianowski, Z. Mazej, P. J. Leszczyński, V. B. Prakapenka, M. Derzsi, V. V. Struzhkin, and W. Grochala, *Inorg. Chem.* **56**, 14651 (2017).
- [14] S. Schyck, E. Evlyukhin, E. Kim, and M. Pravica, *Chem. Phys. Lett.* **724**, 35 (2019).
- [15] See Supplemental Material at <http://link.aps.org/supplemental/10.1103/PhysRevMaterials.8.034407> for complementary data, figures, and structures.
- [16] E. Stavrou, Y. Yao, A. F. Goncharov, Z. Konôpková, and C. Raptis, *Phys. Rev. B* **93**, 054101 (2016).
- [17] C. Kürçü, Z. Merdan, and H. Öztürk, *Russ. J. Phys. Chem.* **90**, 2550 (2016).
- [18] A. Perakis, D. Lampakis, Y. C. Boulmetis, and C. Raptis, *Phys. Rev. B* **72**, 144108 (2005).
- [19] K. Kusaba and T. Kikegawa, *Solid State Commun.* **145**, 279 (2008).
- [20] H. Wang, X. Liu, Y. Li, Y. Liu, and Y. Ma, *Solid State Commun.* **151**, 1475 (2011).
- [21] X. Wu and Z. Wu, *Eur. Phys. J. B* **50**, 521 (2006).
- [22] Z. Mazej, A. Tressaud, and J. Darriet, *J. Fluorine Chem.* **110**, 139 (2001).
- [23] J. Gawraczyński, D. Kurzydłowski, R. A. Ewings, S. Bandaru, W. Gadowski, Z. Mazej, G. Ruani, I. Bergenti, T. Jaroń, A. Ozarowski, S. Hill, P. J. Leszczyński, K. Tokár, M. Derzsi, P. Barone, K. Wohlfeld, J. Lorenzana, and W. Grochala, *Proc. Natl. Acad. Sci. USA* **116**, 1495 (2019).
- [24] R. Piombo, D. Jezierski, H. P. Martins, T. Jaroń, M. N. Gastiasoro, P. Barone, K. Tokár, P. Piekarczyk, M. Derzsi, Z. Mazej, M. Abbate, W. Grochala, and J. Lorenzana, *Phys. Rev. B* **106**, 035142 (2022).
- [25] N. Bachar, K. Koterak, J. Gawraczyński, W. Trzciński, J. Paszula, R. Piombo, P. Barone, Z. Mazej, G. Ghiringhelli, A. Nag, K.-J. Zhou, J. Lorenzana, D. Van Der Marel, and W. Grochala, *Phys. Rev. Res.* **4**, 023108 (2022).
- [26] W. Grochala and R. Hoffmann, *Angew. Chem., Int. Ed.* **40**, 2742 (2001).
- [27] A. Grzelak, M. Derzsi, and W. Grochala, *Inorg. Chem.* **60**, 1561 (2021).
- [28] S. Bandaru, M. Derzsi, A. Grzelak, J. Lorenzana, and W. Grochala, *Phys. Rev. Mater.* **5**, 064801 (2021).
- [29] D. Jezierski, A. Grzelak, X. Liu, S. K. Pandey, M. N. Gastiasoro, J. Lorenzana, J. Feng, and W. Grochala, *Phys. Chem. Chem. Phys.* **24**, 15705 (2022).
- [30] M. A. Domański, M. Derzsi, and W. Grochala, *RSC Adv.* **11**, 25801 (2021).
- [31] D. Jezierski, K. Koterak, M. Domański, P. Połczyński, Z. Mazej, J. Lorenzana, and W. Grochala, *Chem.–A Eur. J.* **29**, e202301092 (2023).
- [32] G. Kresse and J. Furthmüller, *Phys. Rev. B* **54**, 11169 (1996).
- [33] J. P. Perdew, A. Ruzsinszky, G. I. Csonka, O. A. Vydrov, G. E. Scuseria, L. A. Constantin, X. Zhou, and K. Burke, *Phys. Rev. Lett.* **100**, 136406 (2008).
- [34] P. E. Blöchl, *Phys. Rev. B* **50**, 17953 (1994).
- [35] G. Kresse and D. Joubert, *Phys. Rev. B* **59**, 1758 (1999).
- [36] A. I. Liechtenstein, V. I. Anisimov, and J. Zaanen, *Phys. Rev. B* **52**, R5467 (1995).
- [37] V. I. Anisimov, J. Zaanen, and O. K. Andersen, *Phys. Rev. B* **44**, 943 (1991).
- [38] A. B. Kunz, *Phys. Rev. B* **26**, 2070 (1982).
- [39] S. Grimme, J. Antony, S. Ehrlich, and H. Krieg, *J. Chem. Phys.* **132**, 154104 (2010).
- [40] A. Togo and I. Tanaka, *Scr. Mater.* **108**, 1 (2015).
- [41] P. Fischer, W. Hälg, D. Schwarzenbach, and H. Gamsjäger, *J. Phys. Chem. Solids* **35**, 1683 (1974).
- [42] K. Tokár, M. Derzsi, and W. Grochala, *Comput. Mater. Sci.* **188**, 110250 (2021).
- [43] A. Jesih, K. Lutar, B. Žemva, B. Bachmann, St. Becker, B. G. Müller, and R. Hoppe, *Z. Anorg. Allg. Chem.* **588**, 77 (1990).
- [44] W. Grochala, R. G. Egdell, P. P. Edwards, Z. Mazej, and B. Žemva, *ChemPhysChem* **4**, 997 (2003).
- [45] C. Miller and A. S. Botana, *Phys. Rev. B* **101**, 195116 (2020).
- [46] H. Eskes and G. A. Sawatzky, *Phys. Rev. Lett.* **61**, 1415 (1988).
- [47] R. G. Pearson, *Acc. Chem. Res.* **26**, 250 (1993).
- [48] A. Grzelak, H. Su, X. Yang, D. Kurzydłowski, J. Lorenzana, and W. Grochala, *Phys. Rev. Mater.* **4**, 084405 (2020).
- [49] P. Fischer, G. Roullet, and D. Schwarzenbach, *J. Phys. Chem. Solids* **32**, 1641 (1971).
- [50] R. J. Joenk and R. M. Bozorth, *J. Appl. Phys.* **36**, 1167 (1965).
- [51] P. Reinhardt, I. de P. R. Moreira, C. de Graaf, R. Dovesi, and F. Illas, *Chem. Phys. Lett.* **319**, 625 (2000).
- [52] J. B. Goodenough, *Phys. Rev.* **100**, 564 (1955).
- [53] J. Kanamori, *J. Phys. Chem. Solids* **10**, 87 (1959).
- [54] P. W. Anderson, *Phys. Rev.* **79**, 350 (1950).
- [55] I. de P. R. Moreira, D. Muñoz, F. Illas, C. de Graaf, and M. A. Garcia-Bach, *Chem. Phys. Lett.* **345**, 183 (2001).
- [56] D. I. Khomskii, *Transition Metal Compounds* (Cambridge University Press, Cambridge, UK, 2014).
- [57] S. Hayami, Y. Yanagi, and H. Kusunose, *J. Phys. Soc. Jpn.* **88**, 123702 (2019).
- [58] I. Mazin, *Phys. Mag.* **17**, 4 (2024).
- [59] I. Mazin, *Phys. Rev. X* **12**, 040002 (2022).
- [60] S. A. Egorov and R. A. Evarestov, *J. Phys. Chem. Lett.* **12**, 2363 (2021).
- [61] J. Sødequist and T. Olsen, [arXiv:2401.05992v1](https://arxiv.org/abs/2401.05992v1).
- [62] <https://www.ccryst.ehu.es>